HHS Public Access

Author manuscript

Dev Biol. Author manuscript; available in PMC 2016 April 15.

Published in final edited form as:

Dev Biol. 2015 April 15; 400(2): 248–257. doi:10.1016/j.ydbio.2015.02.009.

IFT46 plays an essential role in cilia development

Mi-Sun Lee[1,7], **Kyu-Seok Hwang**[1,7], **Hyun-Woo Oh**[2,7], **Kim Ji-Ae**[2], **Hyun-Taek Kim**[1], **Hyun-Soo Cho**[2], **Jeong-Ju Lee**[2], **Je Yeong Ko**[3], **Jung-Hwa Choi**[1], **Yun-Mi Jeong**[1], **Kwan-Hee You**[1], **Joon Kim**[4], **Doo-Sang Park**[2], **Ki-Hoan Nam**[2], **Shinichi Aizawa**[5], **Hiroshi Kiyonari**[5], **Go Shioi**[5], **Jong-Hoon Park**[3], **Weibin Zhou**[6,*], **Nam-Soon Kim**[2,*], and **Cheol-Hee Kim**[1,*]

[1]Department of Biology, Chungnam National University, Daejeon 305-764, Korea

[2]Korea Research Institute of Bioscience and Biotechnology, Daejeon 305-806, Korea

[3]Department of Biological Science, Sookmyung Women's University, Seoul 140-742, Korea

[4]Graduate School of Medical Science and Engineering, Korea Advanced Institute of Science and Technology, Daejeon 305-701, Korea

[5]Laboratory for Animal Resources and Genetic Engineering, RIKEN Center for Developmental Biology (CDB), Kobe 650-0047, Japan

[6]Department of Pediatrics and Communicable Diseases, University of Michigan Medical School, Ann Arbor, MI 48109-5646, USA

Abstract

Cilia are microtubule-based structures that project into the extracellular space. Ciliary defects are associated with several human diseases, including polycystic kidney disease, primary ciliary dyskinesia, left-right axis patterning, hydrocephalus and retinal degeneration. However, the genetic and cellular biological control of ciliogenesis remains poorly understood. The IFT46 is one of the highly conserved intraflagellar transport complex B proteins. In zebrafish, *ift46* is expressed in various ciliated tissues such as Kupffer's vesicle, pronephric ducts, ears and spinal cord. We show that *ift46* is localized to the basal body. Knockdown of *ift46* gene results in multiple phenotypes associated with various ciliopathies including kidney cysts, pericardial edema and ventral axis curvature. In *ift46* morphants, cilia in kidney and spinal canal are shortened and abnormal. Similar ciliary defects are observed in otic vesicles, lateral line hair cells, olfactory pits, but not in Kupffer's vesicle. To explore the functions of *Ift46* during mouse development, we have generated *Ift46* knock-out mice. The *Ift46* mutants have developmental defects in brain, neural tube and heart. In particular *Ift46(−/−)* homozygotes displays randomization of the embryo heart looping, which is a hallmark of defective left-right (L/R) axis patterning. Taken together, our results demonstrated that IFT46 has an essential role in vertebrate ciliary development.

*Corresponding authors: Weibin Zhou, weibinz@med.umich.edu; Nam-Soon Kim, nskim37@kribb.re.kr; Cheol-Hee Kim, zebrakim@cnu.ac.kr.

[7]These authors contributed equally to this work.

Keywords

cilia; ciliopathy; IFT; intraflagellar transport; IFT46; KO mouse; L/R defect; zebrafish

Introduction

The cilia are microtubule-based organelles evolutionarily conserved from protozoans to vertebrates. Based on their motility, cilia are generally categorized as motile cilia or primary (sensory, non-motile) cilia. A single primary cilium is found on most types of cells, but the number of motile cilia varies in different cells: some, such as those of the embryonic node, have a single motile cilium, while others (ependymal cells in the adult brain and the bronchial epithelium) have multiple motile cilia (Eggenschwiler and Anderson, 2007; Goetz and Anderson, 2010). The importance of primary and motile cilia in embryonic development and in adult physiological processes is underscored by a broad class of human genetic diseases collectively known as “Ciliopathy”, which manifest a broad range of phenotypic abnormalities due to ciliary dysfunction, including obesity, diabetes, skeletal defects, *situs inversus*, hydrocephalus and polycystic kidney disease (PKD) (Badano et al., 2006; Fliegauf et al., 2007). Recent investigation into the role of cilia during early vertebrate development has connected cilia to multiple signaling pathways and many developmental processes ranging from left-right patterning to kidney cystogenesis (Hamada et al., 2002; Hildebrandt and Otto, 2005; Raya et al., 2006).

Cilia can be structurally divided into sub-compartments including basal body, transition zone, axoneme, ciliary membrane and the ciliary tip (Nigg and Raff, 2009). During ciliary growth, the axoneme is assembled by the addition of new axonemal subunits to its distal tip. Since cilia lack the machinery necessary for protein synthesis, the site of assembly of the axoneme is far from the site of synthesis of axonemal proteins in the cell body (Cole and Snell, 2009; Silverman and Leroux, 2009). This demands the delivery of new axonemal building blocks to their assembly site through the intraflagellar transport (IFT), a conserved process in eukaryotes that assembles, maintains, and disassembles cilia, as well as transduces of cilium-generated signaling. IFT is essential for the development and maintenance of both motile and non-motile sensory cilia. IFT trafficking from the base to the tip of the cilium depends on the microtubules and is associated with two IFT protein complexes, termed IFT-A and IFT-B, which consist of at least 6 and 13 subunits respectively. These IFT proteins are highly conserved across species and are all localized to the cilium, basal body and centrosomes (Rosenbaum and Witman, 2002). In mice, IFT-B is essential for anterograde trafficking, whereas IFT-A is required for retrograde trafficking. Disruption of the kinesin-2 motor or IFT-B blocks cilia formation, while perturbation of retrograde trafficking by disrupting the dynein motor or IFT-A results in short and bulged cilia. These highlight that IFT is indispensable for normal ciliogenesis and maintenance (Scholey, 2003). In addition, IFT has recently attracted intense research interest owing to its association with human disease and developmental abnormalities, including polycystic kidney disease (PKD), hepatic and pancreatic defects, blindness and obesity, skeletal patterning abnormalities as well as *situs inversus* (Pazour and Rosenbaum, 2002; Pazour, 2004).

IFT46 is a core component of the intraflagellar transport machinery and is required for formation of all cilia. As a mammalian homologue of DYF-6 in *Caenorhabditis elegans* (*C. elegans*), which was reported to be an IFT-B subunit in *Chlamydomonas reinhardtii* (*C. reinhardtii*), it is specifically required for transporting outer dynein arms into the flagella (Hou et al., 2007). The IFT46 mutants of *C. reinhardtii* and *C. elegans* are incapable of assembling cilia, demonstrating that IFT46 plays an essential role in ciliogenesis. IFT46 forms a stable trimetric sub-complex within the IFT-B core complex together with IFT52 and IFT88 (Lucker, 2010; Richey and Qin, 2012).

Here we report the characterization of *IFT46* by using two model systems, zebrafish and mouse, to elucidate the expression and function of *IFT46* during vertebrate development. We find enriched expression of *ift46* in ciliated organs during zebrafish embryonic development. In addition, we show that knockdown of *ift46* in zebrafish embryos leads to loss of cilia in various tissues. We also demonstrate that *ift46*, like other IFT subunits, is localized to the basal body in ciliated cells. We have generated knock-out mouse of *Ift46*, which are embryonic lethal at E10.5 and exhibit neural tube defects, cardiac edema and randomized heart looping due to the lack of cilia at the node. Taken together, our results indicate the essential role of IFT46 in vertebrate development.

Results

Overexpression of *IFT46* induces apoptotic cell death

We originally isolated a new cDNA clone *C11orf60* in a large-scale expression screening of human genes in zebrafish embryos. Subsequent sequencing revealed this cDNA encodes the human ortholog of *C. reinhardtii* intraflagellar transport protein 46 (IFT46).

When human *IFT46* was overexpressed following the injection of synthetic mRNA of *IFT46* into one cell stage zebrafish at 100 to 200 pg per embryo, we observed increase of apoptosis in the central nervous system of injected embryos in a dose-dependent manner, as determined by acridine orange (AO) staining (Fig. S1A–B). Previous reports have shown that IFT46 in *C. reinhardtii* is specifically required for transporting outer dynein arms into the flagella (Hou et al., 2007). To better characterize and clarify roles of IFT46 in vertebrate development, we thus performed the functional study of the zebrafish *ift46* gene.

The *ift46* is expressed in ciliated organs

We identified from the zebrafish genomic and expressed sequence tags (EST) databases the zebrafish ortholog of IFT46, which encodes 355 amino acids containing a characteristic IFT B protein 46 C-terminal domain. The zebrafish ift46 protein shares a high level of similarity in the conserved domain to its counterparts in human, mouse and *C. reinhardtii* respectively (Fig. 1). RT-PCR revealed both maternal and zygotic expression of *ift46* as early as at four-cell stage (Fig. S1C). We then characterized the expression pattern of *ift46* during zebrafish early development by whole-mount *in situ* hybridization (Fig. 2). *ift46* was expressed ubiquitously at cleavage, blastula stages and specifically in ciliated tissues at later stages. The *ift46* expression was initially detected in dorsal forerunner cells (DFC), which are the precursors of Kupffer's vesicle (KV) and later in KV at 3-somite stage. By 20–24 hours post

fertilization (hpf), widespread expression of *ift46* was evident within the brain, spinal cord and pronephros. In the pronephric ducts, *ift46* was expressed in a salt and pepper pattern at 24 hpf, which resembles the distribution of multi-ciliated epithelial cells in the pronephros. At 54 hpf, *ift46* expression was detected throughout the olfactory placodes and lateral line organs. Thus *ift46* is specifically expressed in ciliated tissues, suggesting its involvement in ciliogenesis during zebrafish embryonic development.

ift46 morphants develop ciliopathy-related defects

To investigate *ift46* function in ciliogenesis and embryonic development, we used morpholino oligo (MO) targeting the translational start site of *ift46* mRNA to knockdown *ift46* expression in zebrafish embryos. The *ift46* ATG-MO is highly effective in blocking the translation of *ift46* mRNA, as shown by co-injection of the MO and GFP-tagged *ift46* into zebrafish embryos (Fig. S1D–E). When *ift46* was knocked down with this MO, we observed a series of ciliopathy-related phenotypes, including ventral body curvature, pronephric cysts and retinal dysplasia (Fig. 3A–F'). These are typical phenotypes seen in zebrafish defective in cilium motility or assembly, such as a number of zebrafish IFT mutants (Kramer-Zucker et al., 2005; Zhao, 2007). The pronephric cysts developed progressively in *ift46* morphant embryos from 2 dpf to 5 dpf. We examined the histology of kidney defects in *ift46* morphants (Fig. 3C–D'). The kidney cysts are located in the glomerular tubular region slightly anterior and medial to the pectoral fin. Cross section of *ift46* morphants at 72 hpf revealed large bilateral cysts in the glomerular-tubular region (Fig. 3C and C'). In addition, *ift46* morphants kidney ducts are grossly dilated compared to control embryos (Fig. 3D and D').

We also examined the retinal histology of *ift46* morphants. The photoreceptor outer segment is a specialized primary cilium consisting of microtubule-based axoneme and regular stacks of disks containing opsin for the photo-transduction cascade (Sukumaran, 2009; Tsujikawa, 2004). Although the overall size of the eye was unaffected under light microscopy, histological sections revealed that the photoreceptor outer segment is thinner than wild-type control in *ift46* morphants (Fig. 3E– F').

To demonstrate the specificity of the knockdown, we performed rescue experiments for the *ift46* morphants by co-injection of *ift46* mRNA. Co-injection of zebrafish *ift46* mRNA with ATG-MO completely rescued the injected embryos, with embryos showing a straight body axis, substantially reduced cyst formation and cardiac edema (Fig. S2). In addition, injection of human *IFT46* mRNA also partially rescued *ift46* morphants (Fig. S2C–F), indicating that zebrafish and human orthologs of IFT46 are functionally conserved and IFT46 is likely to have an evolutionarily conserved role in ciliary function.

The IFT46 protein is predicted to have an intraflagellar transport complex B protein 46 c-terminal domain that is highly conserved in mouse and human (Fig. 1). To delineate the functional significance of this structural feature of *ift46*, we generated a series of deletion mutants of *ift46* and tested their activity to rescue *ift46* morphant phenotypes (Fig. S2A). The expression of the C-terminal portion of *ift46* resulted in a significant rescue of the morphant phenotypes, i.e. kidney cysts and pericardial edema (Fig. S2G), but the expression of the C-terminal deletion mutant of *ift46* failed to rescue (Fig. S2H). In addition, the

overexpression of *ift46* ΔN but not *ift46* ΔC in zebrafish embryos led to elevated numbers of apoptotic cells in the brain region. Therefore, we conclude that the C-terminal domain is necessary for *ift46* function.

The *ift46* localizes to the basal body in ciliated cell and controls the number and the length of cilia during zebrafish development

So far, all IFT proteins characterized have been localized to the cilium, basal body and centrosomes (Kunitomo and Iino, 2008). We expressed GFP-tagged zebrafish ift46 in hTERTRPE1 cells to examine its subcellular localization. Double immunostaining against GFP and acetylated α-tubulin, a marker for cilia, showed that GFP-tagged ift46 was primarily localized at the basal body of cilia but not in the cilium (Fig. 3G–J), consistent with previous reports on IFT46 localization in cultured cells and *C. reinhardtii* (Gouttenoire et al., 2007; Hou et al., 2007). To investigate whether *ift46* is required for cilia assembly like the other IFT-B complex subunits, we first examined cilia morphology using acetylated α-tubulin, a cilia-specific marker, in pronephros, otic vesicle, olfactory pits and lateral line of *ift46* morphant embryos. By confocal microscopy we observed a reduction of cilium length in all of these organs in morphants (Fig. 4A–D'). In the pronephric duct, motile cilia in multi-ciliated cells were shorter and disorganized in morphants compared to the controls (Fig. 4A-A'). Presumably the motility of these cilia was abnormal because the same ciliary defects are accompanied by motility defects in other IFT mutant zebrafish, and hence lead to pronephric cysts (Follit et al., 2009; Gerdes et al., 2009; Zariwala et al., 2007). In the otic vesicles, there are two populations of cilia: tether cilia located at the anterior and posterior ends of the ear and a transient population of short cilia that is distributed throughout the otic vesicle lumen (Stooke-Vaughan et al., 2012). In *ift46* morphant embryos, both types of cilia in the otic vesicle are defective in morphant embryos: the tether cilia were shorter and the short cilia were missing (Fig. 4B-B'). The cilia in the olfactory pits were shorter compared to the controls as revealed by immunofluorescence (Fig. 4C-C') as well as scanning electron microscopy (Fig. 4E–F'). The mechanosensory kinocilia of the lateral line hair cells in *ift46* morphant embryos were consistently shorter than those of the controls (Fig. 4D-D'). However, although the number of cilia was greatly reduced in the pronephric ducts, the "9+2" microtubule doublet pattern within these cilia was not affected by the loss of *ift46* function, as shown by transmission electron microscopy (TEM) (Fig. 4G–H'). Taken together, these results suggest that *ift46* plays an essential role in controlling the cilium number and length, but is not required for the structural assembly of the cilium.

In vertebrate embryos, cilia are required for the left-right (LR) axis formation. The Kupffer's vesicle, a fluid-filled structure, is located at the tail bud in the zebrafish embryo and is the functional counterpart of the mammalian node (Essner et al., 2005; Hirokawa et al., 2009; Kreiling et al., 2007; Oteíza et al., 2008). The KV cells contain motile cilia that generate the fluid flow critical for the establishment of laterality in zebrafish. The absence of these cilia or their lack of motility results in LR patterning defects of various visceral organs such as heart, liver and pancreas (Lenhart et al., 2011). We examined a number of asymmetric markers, including left dorsal diencephalon and left heart primordium marker *lefty1*, heart primordium marker *lefty2*, visceral organ marker *foxA3* but did not observe any LR defects in *ift46* morphants (Fig. S3A–E'). We further examined organogenesis of the KV, and cilia

formation in the KV in morphants at the 4-somite stage. The size and shape of the KV, revealed by the expression of *charon*, a marker of KV and antagonist of Nodal signaling for LR patterning, are normal in *ift46* morphants (Fig. S3F-F') and so are the length and number of cilia in the KV (Fig. S3J–K). Thus *ift46* knockdown resulted in neither ciliary defects in the KV nor abnormal development of the organ laterality, presumably due to the maternal expression of *ift46*.

Left–right axis patterning is defective in *Ift46* knock-out mice

To further assess the functional importance of IFT46 during mammalian development, we generated a knock-out mouse model for *Ift46* by homologous recombination strategy. The targeting vector was generated to delete exon 4 of *Ift46* (Fig. 5A). Correctly targeted ES cell clones obtained with the gene-targeting construct were verified by PCR (Fig. 5B). The *Ift46* homozygous mutants could not be detected among new-born mice of *Ift46* heterozygote incrosses, suggesting embryonic lethality of the homozygotes. By genotyping embryos during gestation, we found that homozygous embryos died between E10.0 and E10.5. In fact, the *Ift46* homozygotes at E9.5 were phenotypically abnormal with severe developmental defects including growth retardation, abnormal neural tube morphology, abnormal cardiac morphology and hemorrhage (Fig. 6A). Their neural tube failed to close and severe cardiac edema was observed at E10.5. *In situ* hybridization revealed that *Ift46* was widely expressed in whole embryo at E10.5 with strong expression especially in the forebrain and the neural tube (Fig. S4D). These expression patterns are in accordance with the mutant phenotypes, which suggest an important role of *Ift46* in neural tube development.

The randomized turning process of the heart tube and abnormal heart looping are observed in the *Ift57* and *Ift88* mutant embryos (Follit et al., 2009; Gorivodsky et al., 2009; Houde et al., 2006; Murcia et al., 2000; Taulman et al., 2001). We examined heart looping orientation in *Ift46* mutant embryos. A various degree of pericardial edema was observed in all *Ift46* homozygous embryos with inverted heart looping. When a clutch of mouse fetus was examined at E9.5, two out of nine showed heart looping defects: one had a linear heart tube and the other showed left-right reversed heart looping (*situs* ambiguous). This suggests that the *Ift46* mutants are defective in left-right axis patterning (Fig. 6B–C). The left-right axis formation is established after the node formation in early-stage embryos. We examined the left-right patterning defect in early embryonic stages by whole-mount *in situ* hybridization of *Lefty-1*, the target of Nodal signaling. In wild-type, *Lefty-1* is expressed on the left side of the lateral plate mesoderm (LPM) at E8.5 (Fig. 6D). By contrast, *Ift46* homozygous mutants showed ectopic bilateral expression of *Lefty-1* (Fig. 6E). These results indicated that *Ift46* is important for LR axis patterning specification in mouse development. The break in LR asymmetry in the mouse is related to the fluid flow towards the left side of the embryo generated by the beating cilia at the node (Houde et al., 2006). To determine whether ciliogenesis is abolished in *Ift46* mutants, we investigated the integrity of the mouse nodal cilia. Scanning electron microscopy of E8.0 embryos showed that *Ift46* homozygous mutants exhibited a depression with similar location and gross morphology to the wild-type node (Fig. 6F and H). At higher magnification, however, we could not observe any monocilia in mutant node cells (Fig. 6G and I). Therefore, absence of nodal flow due to the loss of nodal cilia is the cause of the severe LR patterning defects seen in *Ift46* homozygous mutants.

Discussion

Recent studies of ciliopathy highlight the critical role of cilia in the pathogenesis of multiple ciliated organs such as kidney, respiratory tracts, heart, retina and brain (Fliegauf et al., 2007; Novarino et al., 2011). However, it is still largely unclear how cilia play such an indispensible role in regulating normal organ development and function. Studies of IFT complexes in many model systems such as zebrafish and mice have shown that these proteins are essential for ciliary development. Previous studies about IFT46, an IFT-B complex protein, primarily focused on ciliogenesis in *C. reinhardtii* and *C. elegans*. Here, we described for the first time the functional role of IFT46 in ciliogenesis by using vertebrate models. We isolated zebrafish ortholog of *ift46* and showed that its expression is highly restricted in multiple ciliated tissues, which suggests the diverse functions of *ift46* in embryonic development and organogenesis.

By overexpressing *ift46-GFP* construct in hTERT-RPE1 ciliated cells, we have confirmed the localization of ift46 at the basal body of primary cilia. Consistently, mouse Ift46 has been localized to the base of the primary cilia of mouse chondrocytes with a polyclonal antibody against Ift46 (Gouttenoire et al., 2007; Hou et al., 2007). Proteins required for intraflagellar transport concentrate at the basal body of cilia, where they assemble into protein complexes called IFT particles (Rosenbaum and Witman, 2002). The subcellular localization of ift46 in basal body suggests that IFT46 is indeed involved in IFT process. It is notable that the ift46-GFP fusing protein was not detected within the cilia, differing from the previously report for mouse Ift46, which was detected in primary cilium by an antibody (Gouttenoire et al., 2007). Presumably, the GFP moiety may have interfered with the transport of ift46-GFP into the cilia.

Loss of other IFT B complexes subunits, such as *ift57, ift88* and *ift172*, by mutations or morpholino knockdown has been reported to affect ciliogenesis in zebrafish. In these animal models, both sensory cilia in neurons and motile cilia in the pronephric duct are disrupted (Essner et al., 2005; Lunt et al., 2009). *ift46* morphant zebrafish indeed display most of these cilia biogenesis defects and the morphology of cilia is broadly affected by the loss of IFT46, which confirms that IFT46 is required for the formation of cilia. This notion is corroborated by the consistent ciliary defects discovered in the KO mice of *Ift46* that we have generated. It is noteworthy that the phenotype of *ift46* morphant we observed is different from what was previously published. Gouttenoire *et al.* reported knockdown of *ift46* resulted in dorsalization of developing zebrafish embryos without mentioning any cilium-specific phenotype (Gouttenoire et al., 2007). The discrepancy could be due to the different *ift46* cDNA sequence they isolated, which is shorter than the *ift46* full-length cDNA that we identified using human *IFT46* full-length cDNA. As a consequence, we used different *ift46* morpholino target sites to knock down the gene. Thus whether any alternative coding sequences of *ift46* exist in zebrafish deserves further investigation.

In the absence of IFT, cilia become significantly shorter and have defects in their axonemal microtubules (Kramer-Zucker et al., 2005; Sukumaran, 2009; Tsujikawa, 2004). Indeed, we observed loss of *ift46* led to dramatic shortening or loss of cilia in many ciliated organs including olfactory placode, pronephric duct, ear and lateral line organs, as revealed by

immunohistochemistry and TEM. Despite the reduced ciliary length in various organs, the motile pronephric cilia in *ift46* morphant maintained a normal 9+2 microtubule doublet structures. These results suggest that *ift46* is required for ciliogenesis in ciliated organs but is not essential for axonemal dynein assembly in zebrafish.

Similar to other cilium associated proteins, IFT46 protein domain structure reveals little regarding its function. The only predicted domain in IFT46 is a C-terminal domain conserved in many organisms. Through serial deletion analysis, we showed that C-terminal domain is necessary for ift46 function in normal heart and kidney development, while N-terminal region is dispensable. This result is consistent with our observation that the C-terminal region is highly conserved between multiple species, whereas the N-terminal region is less conserved. Identification of proteins that directly interact with the C-terminal region of IFT46 will provide critical insights to the molecular mechanisms underlying IFT46 functions.

The left-right asymmetry defect is commonly associated with ciliary mutant zebrafish (Essner et al., 2005). Although we observed strong expression of *ift46* in KV, neither the number nor the length of cilia was affected in *ift46* morphants and hence no L-R asymmetry defect. It is likely that the maternal contribution of *ift46* transcript delivers sufficient ift46 protein in the KV. This hypothesis is supported by previous studies of *ift88/ovl* mutants, which exhibit only partial or late loss of cilia, owing to the maternal contribution of this ciliary component. To completely eliminate *ift88* activity, maternal-zygotic *ovl* mutants (MZ*ovl*) was generated using the germline replacement, which showed complete lack of cilia in developing embryos (Huang et al., 2009). Similarly maternal zygotic mutants of *talpid3* also exhibited a curled body and disruption of primary ciliogenesis phenotypes (Ben et al., 2011). The generation and analysis of maternal zygotic *ift46* mutants in the future should provide definitive answer to this possibility. Indeed, we found that the KO mice of *Ift46* displayed severe laterality defects and the ciliary signaling at the node was abnormal, confirming that *Ift46* is indispensible for nodal signaling and laterality control in mouse embryonic development.

Cilia dysfunction has long been associated with cyst formation and ciliopathies. Kidney cysts are thought to be derived from cell over-proliferation with abnormal cellular rearrangement and defects in ciliogenesis and ciliary function can lead to epithelial over proliferation and eventual cyst formation (Sullivan-Brown et al., 2008; Kishimoto et al., 2008). However, how the ciliary signal is coupled to cell proliferation control is poorly understood. We initially isolated IFT46 from an overexpression screening of a human full-length cDNA library, in which overexpressed of IFT46 in zebrafish embryos caused excessive apoptotic cell death. A similar phenomenon has been previously reported for IFT88, of which over-expression prevents G1-S transition and induces apoptotic cell death (Robert et al., 2007; Delaval et al., 2011). In fact, three of the core B subunits, IFT88, IFT52 and IFT46, interact directly with each other and are capable of forming a ternary complex (Lucker et al., 2010). It is notable that IFT46 protein level is high throughout S/M phase and IFT46 regulates the cell cycle progression in together with IFT27 (Wood et al., 2012). Therefore our results suggest that IFT46 might play a potential role in the cell cycle

regulation along with IFT88 and other IFT components. Further work is required to test whether the IFT46 is involved in cell cycle regulation and cytogenesis.

Recently, genome engineering tools (such as ZFN, TALEN and CRISPR) have been successfully developed for targeted mutagenesis (Cho et al., 2013; Sung et al., 2014). This will facilitate the generation of *ift46* and other ciliary mutant lines in zebrafish, which will benefit the functional study of ciliary proteins, such as IFT subunits, and provide animal models for ciliopathy disease genes. Furthermore, characterization of the *ift46* mutations and its interactions with other proteins involved in ciliary formation in development and cell cycle control will deepen our understanding of its function within and outside cilia.

Materials & Methods

Zebrafish maintenance

Zebrafish were maintained at 28.5°C with a 14h light/10h dark condition. Wild-type embryos were cultured in Ringer's solution (116 mM NaCl, 2.9 mM KCL, 1.8 mM $CaCl_2$, 5 mM HEPES, pH 7.2) and treated with PTU (phenylthiocarbamide, 1-Phenyl-2-thiourea) (Sigma) to suppress pigmentation. Embryonic stages were determined by the hours post-fertilization (hpf) and microscopic observation of gross morphology.

Overexpression of *IFT46* in zebrafish embryos

The human *IFT46* clone was a gift from Korea Human Gene Bank, KRIBB. To transcribe the mRNA, the clone was linearized with NotI restriction enzyme and in vitro transcribed by SP6 MESSAGE MACHINE kit (Ambion). The integrity of synthetic mRNA was tested on 1% agarose gel and then dissolved in nuclease-free water. 0.2% phenol red was added immediately before microinjection.

Detection of apoptotic cells

For detection of apoptotic cells, embryos were placed in 10μg/ml acridine orange (Sigma) diluted in egg water for 30 min in dark condition and then washed in egg water.

Cloning of *ift46*

To clone zebrafish *ift46*, a cDNA fragment from 24 hpf zebrafish cDNA was amplified by RT-PCR based on the sequence information on the NCBI sequence (GeneBank ID:XM_003199365.1). The primers were 5'-TCCATGGAGAGGTCCAGACGAC-3' (forward) and 5'-GTCTAGAAATAGGGCAAAAGGGCGACC-3' (reverse). The PCR products were cloned into the pGEM-T easy vector (Promega) and then subcloned into the EcoRI site in pCS2. To construct the *ift46-GFP* fusion reporter into pCS2+ GFP vector, *ift46* was amplified by PCR and the PCR products were subcloned into the NcoI site in pCS2+ GFP vector. The *ift46* ΔN, ΔC constructs were generated using PCR-mediated deletion.

Whole-mount *in situ* hybridization

To make an anti-sense RNA probe (*ift46, foxA3, cmlc2, lefty1, lefty2* and *charon*), the cDNAs were subcloned into the pGEM T-easy vector (Promega), linearized with a

restriction enzyme, and then transcribed *in vitro* using SP6 or T7 polymerase and digoxigenin-labeled UTP (Roche). Whole-mount *in situ* hybridization was performed using standard protocols.

Whole-mount immunostaining

Embryos at the designated stages were fixed in 4% paraformaldehyde. After several washes with PBS, embryos were dehydrated with methanol. Whole-mount immunostaining was carried out as previously described using primary antibodies against mouse acetylated α-tubulin (Sigma). To stain nuclei, the embryos were fixed in 4% paraformaldehyde, stained for 10 min with Hoechst 33342 (Sigma) and washed in PBS.

Microinjection of Morpholino and mRNA

ift46 ATG-MO (Gene Tools) used to blocking translation of *ift46* is 5'-CTTTTGTCGCTCGGACCTCTCCATG-3'. ATG-MO was resuspended in 1X Danieau buffer (58 mM NaCl, 0.7 mM KCl, 0.4 mM $MgSO_4$, 0.6mM $Ca(NO_3)_2$, 5.0 mM HEPES, pH 7.6) with 0.1% phenol red and microinjected into zebrafish embryos at one to four-cell stage (1ng/embryo) using (WPI). Injected embryos were incubated until the indicated stage and analyzed by whole-mount *in situ* hybridization or immunostaining. Capped sense RNA encoding *ift46* (lack of MO target sites) was synthesized with SP6 RNA polymerase (Ambion) after linearization of pCS2+*ift46* with NotI. The synthesized capped RNA was dissolved in nuclease-free water containing 0.2% phenol red as a tracking dye.

Histology

Embryos fixed at 4 dpf in 4% paraformaldehyde were dehydrated with a graded ethanol series up to 100%, processed in xylene and embedded in paraffin. Transverse sections (6μm) were stained with hematoxylin and eosin (H&E) using a standard protocol.

Cell culture and transfection

hTERT-RPE1 cells were grown in DMEM/F12 supplemented with 10% fetal bovine serum, 1% penicillin-streptomycin at 37°C in 5% CO_2, transfected with Lipofectamine™ Reagent (Invitrogen) and serum-starved for 48h to induce ciliogenesis.

Immunostaining and microscopy

hTERT-RPE1 cells grown on glass coverslips were fixed with 4% PFA, permeabilized with 0.1% Triton X-100 in PBS and blocked with 2% horse serum in PBS. Cells were incubated in primary antibody (acetylated α-tubulin, 1/1000) for 1 hour at room temperature and washed three times with PBS and were incubated in fluorescent-conjugated secondary antibodies (1/500) for 1 hour, washed three times with PBS and mounted using DABCO. Confocal imaging was carried out on LSM5 LIVE CONFIGURATION VARIOTWO VRGB confocal microscope.

Scanning electron microscopy (SEM) and Transmission electron microscopy (TEM)

Embryos were fixed with 2.5% glutaraldehyde for 4°C overnight, post-fixed in 1% OsO_4 for 2 hours, dehydrated in a graded series of ethanol. Zebrafish embryos were prepared for TEM and SEM using a standard protocol.

Generation of *Ift46* mutant mice and genotyping

Ift46 mutant mice (Acc. No. CDB0892K: http://www.clst.riken.jp/arg/mutant%20mice%20list.html) were generated as described (http://www.cdb.riken.jp/arg/Methods.html). The targeting vector contains two *loxP* sites and a neomycin resistance cassette for selection in embryonic stem (ES) cells. For gene targeting, ES cell screening and chimera production were carried out. The chimeric mice were mated with C57BL/6 mice to generate F1 heterozygotes. We obtained F1 hetero mice (female 5, male 2 and female 3, male 2) from #91 and #31 ES clones. Genomic DNA was isolated from the mouse ear punched tissues and yolk sac for genotyping. *Ift46* mutant mouse alleles were genotyped by allele-specific PCR with the following primers: *Ift46* (reverse primer) 5'-TGCTACGATCTACTCCCAGACATGC-3'. *Ift46* (WT primer) 5'-AACGATGATGATGACGACGA-3', *Ift46* (MT primer) 5'-CTGACCGCTTCCTCGTGCTTTACG-3'. Primer set of *Ift46* (reverse) and *Ift46* (WT) yields a product of 161 bp and primer set of *Ift46* (reverse), *Ift46* (MT) yields a product of 620 bp. All mouse work conforms to the regulatory standards for experimental animal work as set out by the legal authorities.

Phenotyping of mice

To analyze mouse embryonic phenotypes, crosses of heterozygous mice are set up and vaginal plugs are checked each morning to establish the day of conception. After dissection of female mice, the thin amniotic membrane surrounding embryos was removed, and embryos were fixed in 4% paraformaldehyde. Whole-mount *in situ* hybridizations was performed using standard protocols.

Histology of mouse embryos

Mouse embryonic brains were fixed in 4% paraformaldehyde solution at room temperature overnight. Specimens were dehydrated and embedded in paraffin. Serial sections (thickness of 6 μm) were prepared.

Scanning Electron Microscopy (SEM) of mouse embryos

Embryos at E8.0 were dissected in PBS with 0.05% Triton X-100 and fixed overnight in 2.5% PFA, 2.5% glutaraldehyde in 0.075M sodium cacodylate buffer, pH 7.4. Embryos are placed in 100% ethanol for critical point drying using E3000 (Polaron) critical point dryer. Critical point dried embryos were placed on a piece of carbon tape and sputter coated with gold in a SC7640 Sputter Coater. Specimens were imaged on a Quanta 250 Field Emission Scanning Electron microscope (FEI).

Supplementary Material

Refer to Web version on PubMed Central for supplementary material.

Acknowledgments

Funding

This research was supported by the Basic Science Research Program (20100024645), the KRIBB Research Initiative Program (KGM4611411) and the Bio & Medical Technology Development Program (2012M3A9D1054519 for J.-H.P. and 2014M3A9A5034156 for N.-S. K.) of the National Research Foundation (NRF) funded by the Ministry of Science, ICT & Future Planning. W. Z. is supported by NIH grants (R00DK091405 and P30DK081943) and Carl W. Gottschalk Research Scholar Grant from the American Society of Nephrology.

References

Badano J, Mitsuma N, Beales P, Katsanis N. The ciliopathies: an emerging class of human genetic disorders. Annu. Rev. Genomics Hum. Genet. 2006; 7:125–148. [PubMed: 16722803]

Ben J, Elworthy S, Ng AS, van Eeden F, Ingham PW. Targeted mutation of the talpid3 gene in zebrafish reveals its conserved requirement for ciliogenesis and Hedgehog signalling across the vertebrates. Development. 2011; 138:4969–4978. [PubMed: 22028029]

Cho S, Kim S, Kim J, Kim J-S. Targeted genome engineering in human cells with the Cas9 RNA-guided endonuclease. Nat. Biotechnol. 2013; 31:230–232. [PubMed: 23360966]

Cole D, Snell W. SnapShot: Intraflagellar transport. Cell. 2009; 137:784–784.e1. [PubMed: 19450523]

Delaval B, Bright A, Lawson N, Doxsey S. The cilia protein IFT88 is required for spindle orientation in mitosis. Nat. Cell Biol. 2011; 13:461–468. [PubMed: 21441926]

Eggenschwiler J, Anderson K. Cilia and developmental signaling. Annu. Rev. Cell Dev. Biol. 2007; 23:345–373. [PubMed: 17506691]

Essner J, Amack J, Nyholm M, Harris E, Yost H. Kupffer's vesicle is a ciliated organ of asymmetry in the zebrafish embryo that initiates left-right development of the brain, heart and gut. Development. 2005; 132:1247–1260. [PubMed: 15716348]

Fliegauf M, Benzing T, Omran H. When cilia go bad: cilia defects and ciliopathies. Nat. Rev. Mol. Cell Biol. 2007; 8:880–893. [PubMed: 17955020]

Follit JA, Xu F, Keady BT, Pazour GJ. Characterization of mouse IFT complex B. Cell Motil. Cytoskeleton. 2009; 66:457–468. [PubMed: 19253336]

Gerdes J, Davis E, Katsanis N. The vertebrate primary cilium in development, homeostasis, and disease. Cell. 2009; 137:32–45. [PubMed: 19345185]

Goetz S, Anderson K. The primary cilium: a signalling centre during vertebrate development. Nat. Rev. Genet. 2010; 11:331–344. [PubMed: 20395968]

Gorivodsky M, Mukhopadhyay M, Wilsch-Braeuninger M, Phillips M, Teufel A, Kim C, Malik N, Huttner W, Westphal H. Intraflagellar transport protein 172 is essential for primary cilia formation and plays a vital role in patterning the mammalian brain. Dev. Biol. 2009; 325:24–32. [PubMed: 18930042]

Gouttenoire J, Valcourt U, Bougault C, Aubert-Foucher E, Arnaud E, Giraud L, Mallein-Gerin F. Knockdown of the intraflagellar transport protein IFT46 stimulates selective gene expression in mouse chondrocytes and affects early development in zebrafish. J. Biol. Chem. 2007; 282:30960–30973. [PubMed: 17720815]

Hamada H, Meno C, Watanabe D, Saijoh Y. Establishment of vertebrate left-right asymmetry. Nat. Rev. Genet. 2002; 3:103–113. [PubMed: 11836504]

Hildebrandt F, Otto E. Cilia and centrosomes: a unifying pathogenic concept for cystic kidney disease? Nat. Rev. Genet. 2005; 6:928–940. [PubMed: 16341073]

Hirokawa N, Tanaka Y, Okada Y. Left-right determination: involvement of molecular motor KIF3, cilia, and nodal flow. Cold Spring Harb Perspect Biol. 2009; 1:a000802. [PubMed: 20066075]

Hou Y, Qin H, Follit J, Pazour G, Rosenbaum J, Witman G. Functional analysis of an individual IFT protein: IFT46 is required for transport of outer dynein arms into flagella. J. Cell Biol. 2007; 176:653–665. [PubMed: 17312020]

Huang P, Schier AF. Dampened Hedgehog signaling but normal Wnt signaling in zebrafish without cilia. Development. 2009; 136:3089–3098. [PubMed: 19700616]

Houde C, Dickinson R, Houtzager V, Cullum R, Montpetit R, Metzler M, Simpson E, Roy S, Hayden M, Hoodless P, Nicholson D. Hippi is essential for node cilia assembly and Sonic hedgehog signaling. Dev. Biol. 2006; 300:523–533. [PubMed: 17027958]

Kishimoto N, Cao Y, Park A, Sun Z. Cystic kidney gene seahorse regulates cilia-mediated processes and Wnt pathways. Dev. Cell. 2008; 14:954–961. [PubMed: 18539122]

Kramer-Zucker A, Olale F, Haycraft C, Yoder B, Schier A, Drummond I. Cilia-driven fluid flow in the zebrafish pronephros, brain and Kupffer's vesicle is required for normal organogenesis. Development. 2005; 132:1907–1921. [PubMed: 15790966]

Kreiling J, Williams G, Creton R. Analysis of Kupffer's vesicle in zebrafish embryos using a cave automated virtual environment. Dev. Dyn. 2007; 236:1963–1969. [PubMed: 17503454]

Kunitomo H, Iino Y. Caenorhabditis elegans DYF-11, an orthologue of mammalian Traf3ip1/MIP-T3, is required for sensory cilia formation. Genes Cells. 2008; 13:13–25. [PubMed: 18173744]

Lenhart K, Lin S-Y, Titus T, Postlethwait J, Burdine R. Two additional midline barriers function with midline lefty1 expression to maintain asymmetric Nodal signaling during left-right axis specification in zebrafish. Development. 2011; 138:4405–4410. [PubMed: 21937597]

Lucker B, Miller M, Dziedzic S, Blackmarr P, Cole D. Direct interactions of intraflagellar transport complex B proteins IFT88, IFT52, and IFT46. J. Biol. Chem. 2010; 285:21508–21518. [PubMed: 20435895]

Lunt SC, Haynes T, Perkins BD. Zebrafish ift57, ift88, and ift172 intraflagellar transport mutants disrupt cilia but do not affect hedgehog signaling. Dev Dyn. 2009; 238:1744–1759. [PubMed: 19517571]

Murcia N, Richards W, Yoder B, Mucenski M, Dunlap J, Woychik R. The Oak Ridge Polycystic Kidney (orpk) disease gene is required for left-right axis determination. Development. 2000; 127:2347–2355. [PubMed: 10804177]

Nigg E, Raff J. Centrioles, centrosomes, and cilia in health and disease. Cell. 2009; 139:663–678. [PubMed: 19914163]

Novarino G, Akizu N, Gleeson J. Modeling human disease in humans: the ciliopathies. Cell. 2011; 147:70–79. [PubMed: 21962508]

Oteíza P, Köppen M, Concha M, Heisenberg C-P. Origin and shaping of the laterality organ in zebrafish. Development. 2008; 135:2807–2813. [PubMed: 18635607]

Pazour G, Rosenbaum J. Intraflagellar transport and cilia-dependent diseases. Trends Cell Biol. 2002; 12:551–555. [PubMed: 12495842]

Pazour G. Intraflagellar transport and cilia-dependent renal disease: the ciliary hypothesis of polycystic kidney disease. J. Am. Soc. Nephrol. 2004; 15:2528–2536. [PubMed: 15466257]

Raya A, Izpisúa, Belmonte J. Left-right asymmetry in the vertebrate embryo: from early information to higher-level integration. Nat. Rev. Genet. 2006; 7:283–293. [PubMed: 16543932]

Richey E, Qin H. Dissecting the sequential assembly and localization of intraflagellar transport particle complex B in Chlamydomonas. PLoS One. 2012; 7:e43118. [PubMed: 22900094]

Robert A, Margall-Ducos G, Guidotti JE, Brégerie O, Celati C, Bréchot C, Desdouets C. The intraflagellar transport component IFT88/polaris is a centrosomal protein regulating G1-S transition in non-ciliated cells. J. Cell Sci. 2007; 120:628–637. [PubMed: 17264151]

Rosenbaum J, Witman G. Intraflagellar transport. Nat. Rev. Mol. Cell Biol. 2002; 3:813–825. [PubMed: 12415299]

Silverman M, Leroux M. Intraflagellar transport and the generation of dynamic, structurally and functionally diverse cilia. Trends Cell Biol. 2009; 19:306–316. [PubMed: 19560357]

Scholey J. Intraflagellar transport. Annu. Rev. Cell Dev. Biol. 2003; 19:423–443. [PubMed: 14570576]

Stooke-Vaughan G, Huang P, Hammond K, Schier A, Whitfield T. The role of hair cells, cilia and ciliary motility in otolith formation in the zebrafish otic vesicle. Development. 2012; 139:1777–1787. [PubMed: 22461562]

Sukumaran S, Perkins B. Early defects in photoreceptor outer segment morphogenesis in zebrafish ift57, ift88 and ift172 Intraflagellar Transport mutants. Vision Res. 2009; 49:479–489. [PubMed: 19136023]

Sullivan-Brown J, Schottenfeld J, Okabe N, Hostetter C, Serluca F, Thiberge S, Burdine R. Zebrafish mutations affecting cilia motility share similar cystic phenotypes and suggest a mechanism of cyst formation that differs from pkd2 morphants. Dev. Biol. 2008; 314:261–275. [PubMed: 18178183]

Sung Y, Kim J, Kim H-T, Lee J, Jeon J, Jin Y, Choi J-H, Ban Y, Ha S-J, Kim C-H, Lee H-W, Kim J-S. Highly efficient gene knockout in mice and zebrafish with RNA-guided endonucleases. Genome Res. 2014; 24:125–131. [PubMed: 24253447]

Taulman P, Haycraft C, Balkovetz D, Yoder B. Polaris, a protein involved in left-right axis patterning, localizes to basal bodies and cilia. Mol. Biol. Cell. 2001; 12:589–599. [PubMed: 11251073]

Tsujikawa M, Malicki J. Intraflagellar transport genes are essential for differentiation and survival of vertebrate sensory neurons. Neuron. 2004; 42:703–716. [PubMed: 15182712]

Wood C, Wang Z, Diener D, Zones J, Rosenbaum J, Umen J. IFT proteins accumulate during cell division and localize to the cleavage furrow in Chlamydomonas. PLoS One. 2012; 7:e30729. [PubMed: 22328921]

Zariwala M, Knowles M, Omran H. Genetic defects in ciliary structure and function. Annu. Rev. Physiol. 2007; 69:423–450. [PubMed: 17059358]

Zhao C, Malicki J. Genetic defects of pronephric cilia in zebrafish. Mech. Dev. 2007; 124:605–616. [PubMed: 17576052]

Highlights

- IFT46 over-expression induces apoptosis in developing zebrafish embryos.
- Loss of IFT46 displays typical phenotypes of ciliary defects in both zebrafish and mice.
- IFT46 C-terminal domain is required for IFT46 function.
- IFT46 is not essential for axonemal dynein assembly in zebrafish.

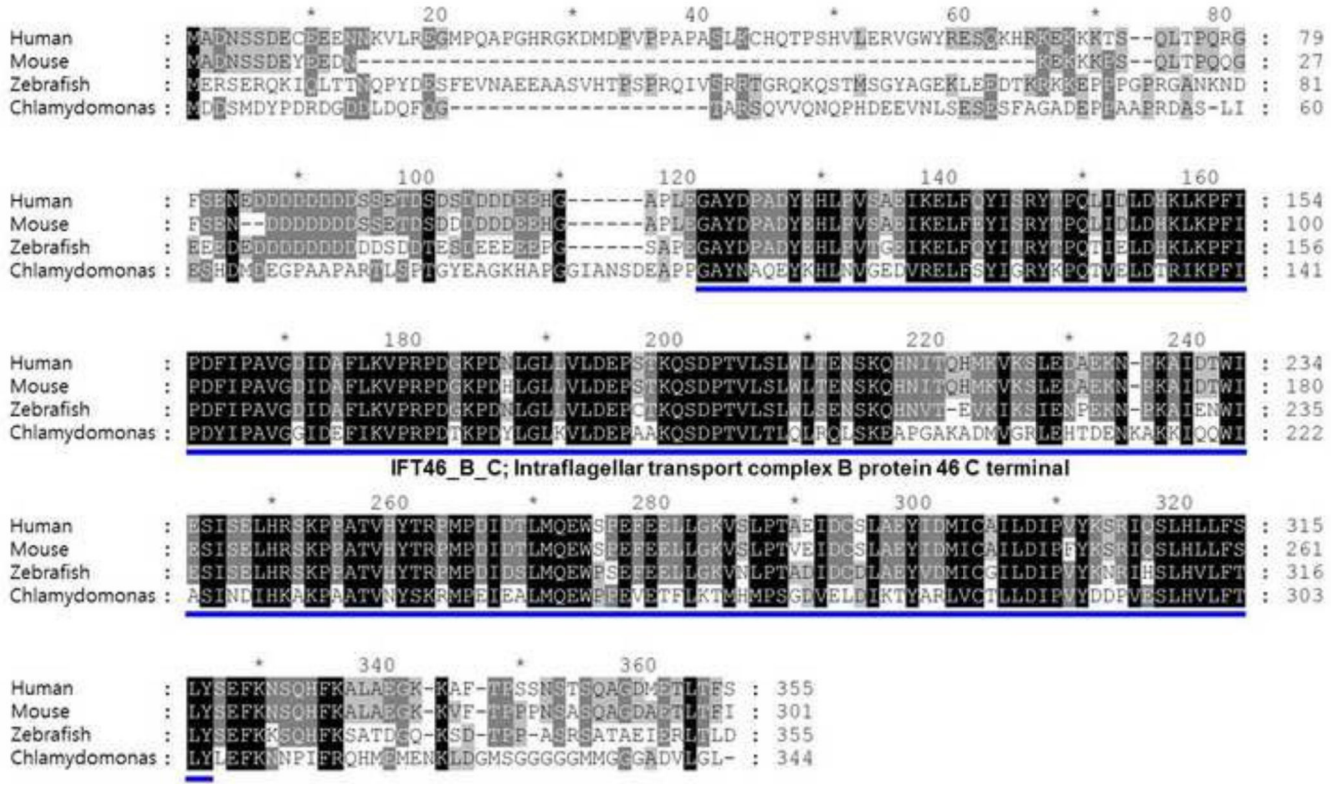

Fig 1. Alignment of IFT46 protein sequences using GeneDoc

The IFT46 protein sequences from human, mouse, zebrafish and Chlamydomonas are aligned using GeneDoc program. The intraflagellar transport complex B protein 46 C terminal domain is marked with blue bar, The zebrafish ift46 has 59%, 69% similarity to human IFT46 and mouse Ift46 and 69% similarity to Chlamydomonas, respectively.

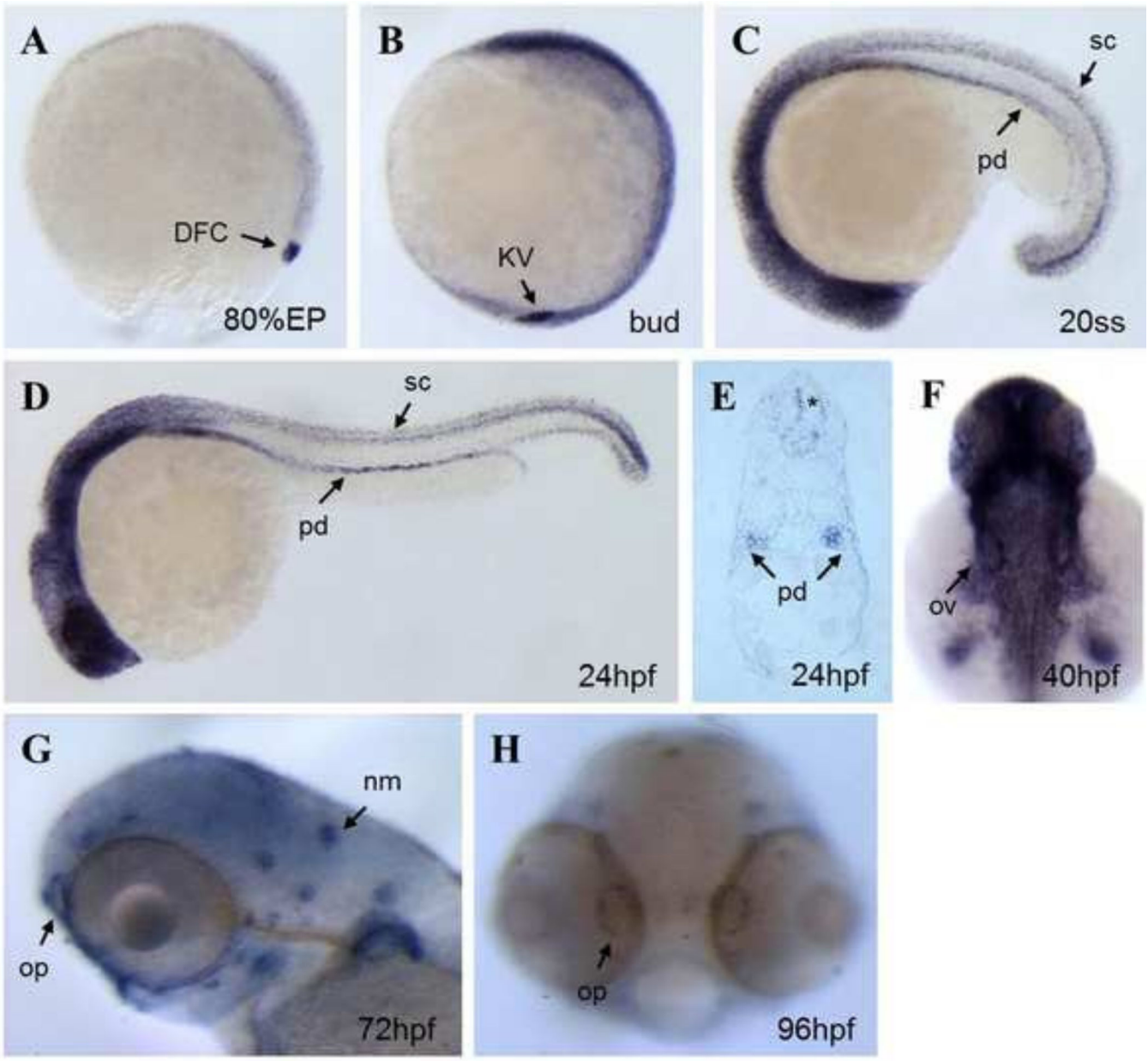

Fig 2. Expression pattern of *ift46* in zebrafish embryos

(A) Whole-mount *in situ* hybridization shows *ift46* expression at 80% epiboly in the dorsal forerunner cells (DFC, arrow). (B) *ift46* is strongly expressed in Kupffer's vesicle (KV, arrow) at bud stage, (C, D) At 20-somite stage and 24 hpf *ift46* expression is detected in pronephric ducts (pd), eyes, ears, spinal cord (sc) and diffusely in the brain. (E) Cross-section showing *ift46* expression in the pronephric ducts (arrow) and spinal cord (asterisk). (F) At 40 hpf, *ift46* is widely expressed in brain, eyes, otic vesicles (arrow) and pectoral fins. (G, H) At 72 and 96 hpf, *ift46* is expressed in the olfactory pits (op) and neuromast (nm) hair cells (arrow).

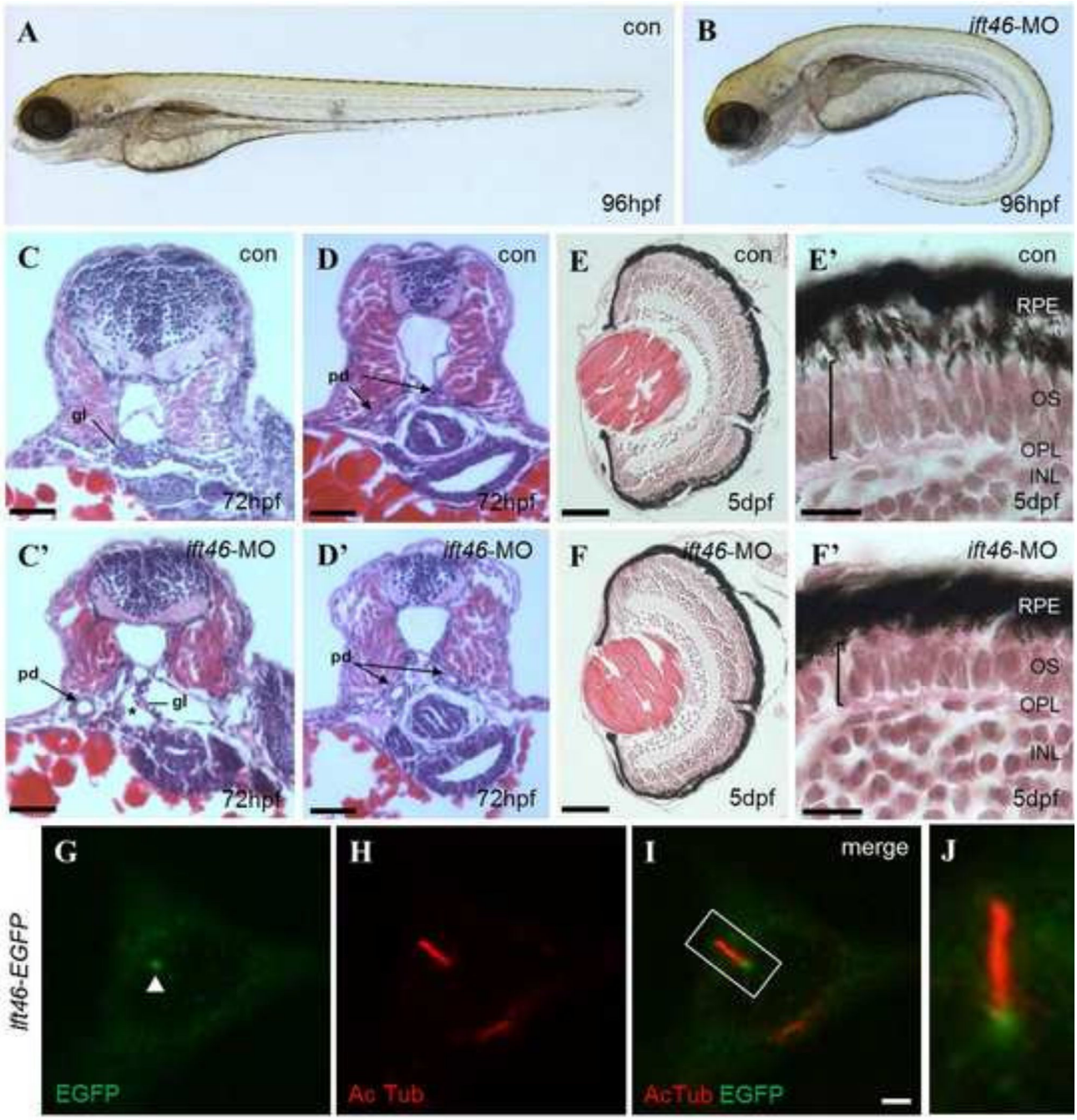

Fig 3. *ift46* morphants develop phenotypes associated with ciliary dysfunction

(A) Wild-type embryos show normal morphology. (B) *ift46* morphants are characterized by curved body axis, the development of pronephric cyst and pericardiac edema at 96 hpf. (C–D) Cross-sections of wild-type zebrafish at the glomerular-tubular region of pronephros at 72 hpf show normal morphology of pronephric glomeruli and ducts. (C'–D') *ift46* morphant embryos display a grossly distended cyst (asterisk) in place of glomeruli (gl) and dilated pronephric ducts (pd) (arrow). Scale bar, 50 μm. (E-F') Histological sections of the eyes of wild-type and *ift46* morphants at 5 dpf. The retina in wild-type control (E and E') has

normal laminated structures, including retinal pigment epithelium (RPE), outer segment (OS), outer plexiform layer (OPL) and inner nuclear layer (INL). (E) and (F) scale bar, 200 μm. The outer segment (OS) (bracket) is thinner in *ift46* morphants (F') compared to the control (E'). Scale bar, 100 μm. (G–J) The EGFP-tagged ift46 (green) is localized to the base of primary cilia (red) in hTERT-RPE1 cells. Merged imaged are shown in (I). Arrowhead indicates the base of cilia. Scale bar, 3 μm. (J) Higher magnification view of the boxed area in (I).

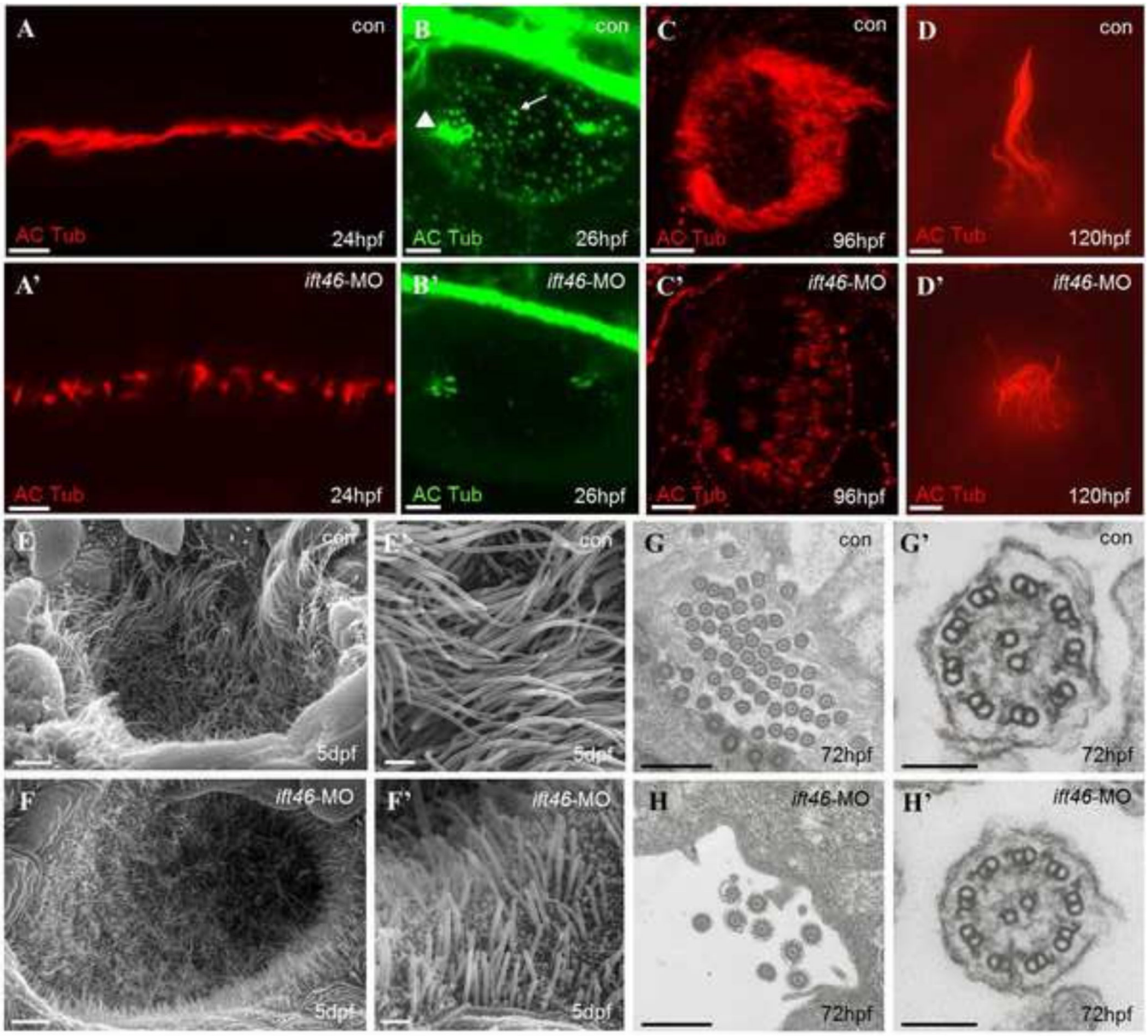

Fig 4. Ciliary defects in zebraifh *ift46* morphants

Immunofluorescence with antibody against acetylated α-tubulin showing cilia in the pronephric ducts, (scale bar, 10 μm) (A-A'), otic vesicle, (scale bar, 10 μm) (B-B'), olfactory placode, (scale bar, 10 μm) (C-C') and a lateral line hair cell, (scale bar, 5 μm) (D-D'). The *ift46* morphants exhibit shortened or fewer cilia compared with the control fish in all of these organs. Arrow head: tether cilia. Arrow: short cilia. (E–F') SEM images showing the cilia in the olfactory placode of control fish (E, E') and *ift46* morphants (F, F') at 5 dpf. Scale bar, 40 μm (E) and (F), 4 μm (E') and (F') (G-H') TEM images of cilia in zebrafish pronephric ducts at 72 hpf. Ultrastructure of normal pronephric cilia shows 9+2 microtubule architecture at 72 hpf which is intact in *ift46* morphants. (G', H') Representative views of individual cilium at higher magnification. Scale bar, 5 μm (G) and (H), 100 μm (G') and (H').

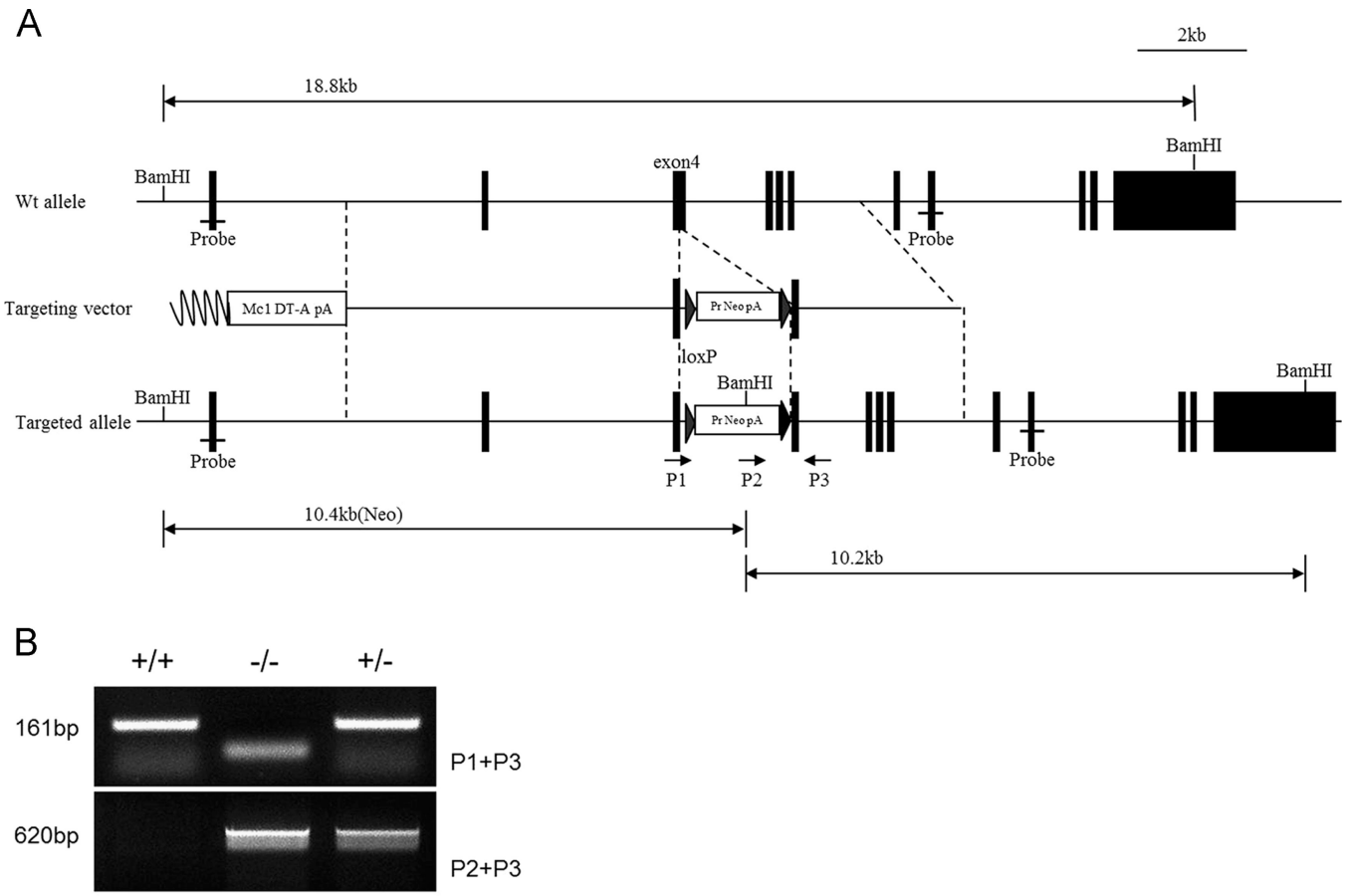

Fig 5. *Ift46* mutant mice were generated by homologous recombination

(A) Schematic diagram indicating the structure of the mouse *Ift46* gene and the gene-targeting strategy. The *Ift46* mutant mice were generated by targeting exon 4. Genotyping primers are shown in the map P1–P3 (arrows). (B) Genotyping of *Ift46* mutants at E9.5. The wild-type allele, *Ift46* WT, produces a 161 bp fragment and the mutated allele, *Ift46* MT, produces a 620 bp PCR fragment.

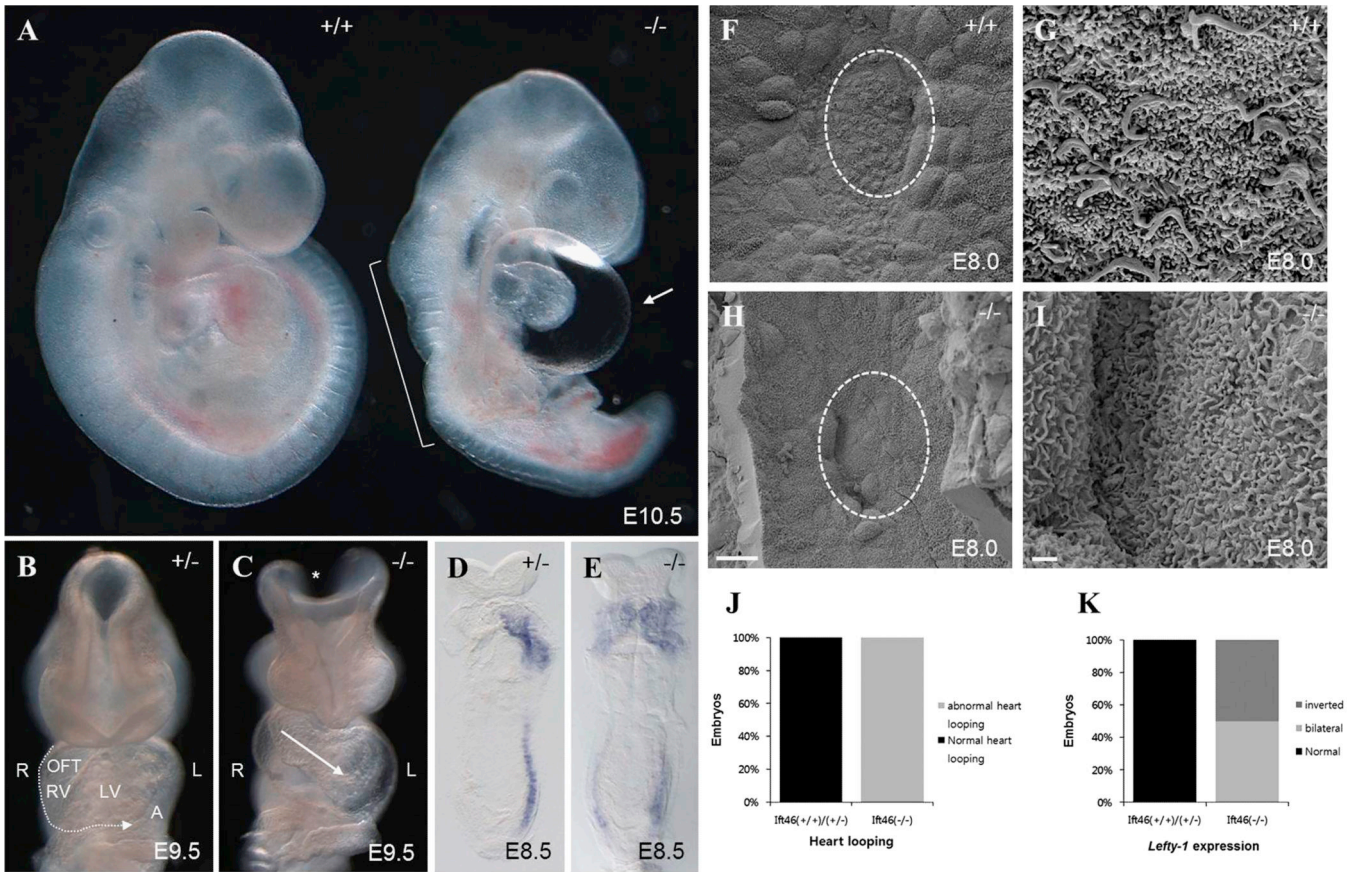

Fig 6. Phenotypic characterization of *Ift46* knock-out mouse embryos

(A) *Ift46* homozygotes exhibit anterior defects, kinks of the neural tube (bracket) and pericardial edema (arrow) at E10.5. (B) At E9.5, normal heart-looping and neural tube closure are seen in heterozygous mice. (C) The cranial neural tube (asterisk) fails to close and the heart looping is abnormal in *Ift46* homozygous (−/−) (arrow). LV, left ventricle; OFT, outflow tract; RV, right ventricle; A, atrial. (D–E) Whole-mount *in situ* hybridization of *Ift46* heterozygous and homozygous mutant embryos for *Lefty-1* detects abnormal bilateral expression of *Lefty-1* in homozygotes. (F–I) Scanning electron microscopy of the embryonic nodal cilia in wild-type (F, G) and *Ift46* homozygous (−/−) embryos (H, I). Ventral view of the E8.0 embryos at 1,500X (F, H) and 10,000X (G, I) magnifications. Anterior to the top. Circle in (F, H) indicates magnified area in (G, I). Scales bars: 20 μm (F, H), 1 μm (G, I). (J) Analysis of mouse heart looping in *Ift46*(+/+) /*Ift46*(+/−) (n=52) and *Ift46*(−/−) (n=9). (K) Analysis of *Lefty-1* expression in E8.5 mouse embryos (*Ift46*(+/+) / *Ift46*(+/−), n=9) (*Ift46*(−/−), n=2).